frontiers in Materials

ORIGINAL RESEARCH
published: 04 March 2021
doi: 10.3389/fmats.2021.633404

Experimental Study of Bond Behavior Between Rebar and PVA-Engineered Cementitious Composite (ECC) Using Pull-Out Tests

Jie Xiao[1], Xiang Long[2], Ming Ye[2], Haibo Jiang[1], Lingfei Liu[3] and Keyi Zhai[1]*

[1]School of Civil and Transportation Engineering, Guangdong University of Technology, Guangzhou, China, [2]Yuexiu Transport Infrastructure Co., Ltd., Hongkong, China, [3]Transportation and Civil Buildings College, Foshan University, Foshan, China

As a novel civil engineering material, Engineered Cementitious Composite (ECC) has attracted more and more attention due to its strain-hardening characteristics, good post-cracking resistance and its unique properties. Bonding between Engineered Cementitious Composite (ECC) and rebar has a great effect on the mechanical behavior of structural members. In this paper, direct pull-out tests were conducted to understand the bond behavior between the ECC and rebar. The test parameters included rebar diameter and type, cover layer thickness, embedment length and fiber volume content. Bond-slip curves, failure and cracking pattern and bond strength were compared and discussed. The test results indicated that the bond strength decreased with the increase of embedded length. Through regression analysis with the test data, the functional relationships between bond strength and cover layer thickness and rebar diameter were fitted well. According to the positive and negative signs of the fitting parameters m and n, the relationship between the bond strength and the cover layer thickness and the rebar diameter could be determined. The bond strength increased obviously with the increase of fiber content. When the fiber volume content was 1, 1.5 and 2%, the bond strength of these specimens were 1.5, 2.5 and 3.1 times that of specimens without polyvinyl alcohol (PVA) fiber.

Keywords: bond-behavior, engineered cementitious composite (ECC), pull-out tests, Embedment length, protective layer thickness

OPEN ACCESS

Edited by:
Shengwen Tang,
Wuhan University, China

Reviewed by:
Kequan Yu,
University of Michigan, United States
Huamei Yang,
Wuchang University of Technology, China
E Chen,
Chalmers University of Technology, Sweden

****Correspondence:***
Haibo Jiang
hbjiang@gdut.edu.cn

Specialty section:
This article was submitted to Structural Materials, a section of the journal Frontiers in Materials

Received: *25 November 2020*
Accepted: *19 January 2021*
Published: *04 March 2021*

Citation:
Xiao J, Long X, Ye M, Jiang H, Liu L and Zhai K (2021) Experimental Study of Bond Behavior Between Rebar and PVA-Engineered Cementitious Composite (ECC) Using Pull-Out Tests. Front. Mater. 8:633404. doi: 10.3389/fmats.2021.633404

INTRODUCTION

Concrete is one of the most widely used and studied building materials in civil engineering projects around the world (Jiang et al., 2016; Xiao et al., 2016; Zhang et al., 2018; Wang et al., 2020a; Wang et al., 2020b; Wang et al., 2020c; Yu et al., 2020a; Wang et al., 2021; Xiong et al., 2021). It has continuously evolved in response to new requirements in field applications since the advent of concrete since 18th century (Li, 2019). Engineered Cementitious Composites (ECC) is a novel civil engineering material consisting primarily of fibers, fine aggregates, cement and admixture. ECC has attracted more and more attention from both researchers and engineers due to its superior strain-hardening behavior and ultra-high strain capacity in uniaxial tension compared to normal concretes (Yu et al., 2020b). As is known to all, good bond property between steel bars and surrounding concrete is critical to ensure that the two materials work together and the bond behavior between steel bars and concrete is the basis for engineering design, numerical analysis, and numerical simulation of reinforced concrete structures (Ma et al., 2017; Nguyen et al., 2020). Even though many

types of research have been conducted to investigate the bond behaviors between steel rebar and concrete (Baena et al., 2009; Shin et al., 2018; Zhou and Qiao, 2018; Pauletta et al., 2020; Rockson et al., 2020), relatively limited investigations have been carried out in order to study the bond strength with reinforcement bars in ECC (Zhou et al., 2019). carried out pull-out tests to consider the effects of ECC strength, steel bar diameter, and the degree of fiber-reinforced polymer (FRP) confinement on steel bar-ECC bonding behavior and proposed a constitutive model to predict the bond-slip behaviors of steel bar-ECC with and without FRP confinement (Lee et al., 2016). conducted pull-out tests to investigate the bond-slip behavior of reinforcement embedded in ECC and found that compared with concrete, ECC could increase the maximum local bond stress of short reinforcement by 14% (Deng et al., 2018). investigated the bond behavior of steel bar embedded in ECC by pull-out test to consider the influence of bar shape, bar diameter, ECC strength, cover thickness and fiber volume content and concluded that the bond stress-slip curves of ECC specimens declined slowly which demonstrated better ductility than that in reinforced concrete (Chao et al., 2009). evaluated the bond strength and the bond stress-slip response of deformed reinforcing bars embedded in fiber-reinforced cementitious composites and revealed that the confinement and bridging effects provided by fibers in FRC composites after cracking could effectively enhance bond strength (Wang et al., 2015). performed pull-out tests to study the effects of the bar diameter, the embedded length, the cover thickness, and the properties of matrix materials on the bond behavior between the basalt fiber reinforced plastic (BFRP) bar and the ECC and concluded that the bridging effect of polyvinyl alcohol (PVA) fibers could enhance the bond performance (Li et al., 2017). investigated the bond performance of steel reinforcing bars embedded in a high-performance fiber-reinforced cementitious composite (HPFRCC) and found that the bond strength decreased with the heating temperature and with the size and embedded length of steel bars (Achara et al., 2019). reported an investigation of the bond performance of the steel reinforcement embedded in nano-silica modified SC-ECC materials through pull-out tests (Hossain et al., 2020). evaluated the bond behavior of GFRP bars embedded in normal concrete and ECCs through 90 pull-out specimens to analyze the effects of bar diameter, bar type, embedment length and concrete type on bond strength and failure modes and confirmed the superior bond characteristics of ECC compared with normal concrete (Bai et al., 2019). investigated the bond behavior of H-shaped steel embedded in engineered cementitious composites (ECC) by changing the volume fraction of polyvinyl alcohol (PVA) fiber, stirrup reinforcement ratio, ECC cover thickness and H-shaped steel embedded length (Cai et al., 2020). studied the bond behaviors of deformed steel rebars in engineered cementitious composite (ECC) and concrete under the direct pull-out condition and found the deformed steel rebar has a much higher bond strength in ECC than in concrete (Kim and Lee, 2012). presented experimental investigations of the interfacial bond behavior of different types of rebar and cementitious composites and found that the increase in PVA fiber volume fraction significantly improved the ductility of the matrix. The bond performance of embedded steel rebar is one of the most important engineering properties for reinforced concrete structures. Therefore, to widen the scope and encourage the use of ECC in structural applications, a reliable characterization of the bond interaction between steel rebar and ECC still need more investigations. This paper presented an experimental study on bond behavior between rebar and engineered cementitious composite (PVA-ECC) using a pull-out test. The test parameters included rebar diameter and type, cover layer thickness, embedment length and fiber volume content. Bond-slip curves, failure and cracking pattern and bond strength were compared and discussed. The present paper was expected to enrich knowledge about the bond behavior between rebar and ECC and to provide reference for the popularization and application of ECC materials in engineering.

TABLE 1 | Mixture proportions for ECC matrix with different fiber volume content.

Materials/kg/m^3	PVA fiber volume content/%			
	0	1	1.5	2
Cement	383.7	383.7	383.7	383.7
Fly ash	895.3	895.3	895.3	895.3
Silica sand	455	455	455	455
Superplasticizer	10.12	10.12	10.12	10.12
PVA fiber	0	13	19.5	26
Water	303	303	303	303

EXPERIMENTAL PROGRAM

Materials

The constituent materials of the ECC mixtures in this study were provided in **Table 1**, including ordinary Portland cement, fly ash, silica sand, polycarboxylate superplasticizer, polyvinyl alcohol (PVA) fiber and water. The average 28-days compressive strength for ECC was 48 MPa. **Table 2** showed the characteristics of PVA fiber used in this study, which was produced by Kuraray Co. Ltd., Japan.

Fresh ECC mixtures were cast into dog-bone shaped molds on a vibration table at a moderate vibration rate. The geometry of dog-bone specimens conforms to JSCE (Cai et al., 2020). Specimens were demolded after 24 h. After demolding, specimens were cured in sealed plastic bags at room temperature (23 ± 3°C) for 7 days and then stored at room temperature until the age of 28 days. At 28 days, uniaxial tensile tests were performed with a servo-hydraulic testing frame, under displacement control (0.5 mm/min). Two external linear variable displacement transducers (LVDT) were attached to the specimen with a gauge length of 100 mm for strain measurement. Design and performance of the adapted ECC in the experiment were shown in **Figure 1**.

Figure 2 gave the tensile stress-strain curves of ECC adopted in this study, which exhibited a strain hardening branch and the maximum tensile strain exceeds 3% when subjected to tensile load. It meant the ECC used in this study showed good toughness

TABLE 2 | Characteristics of PVA fiber.

Density/g/m^3	Diameter/mm	Length/mm	Nominal tensile strength/MPa	Elongation at rupture/%	Young's modulus/GPa
1.3	0.04	12	1,600	6	40

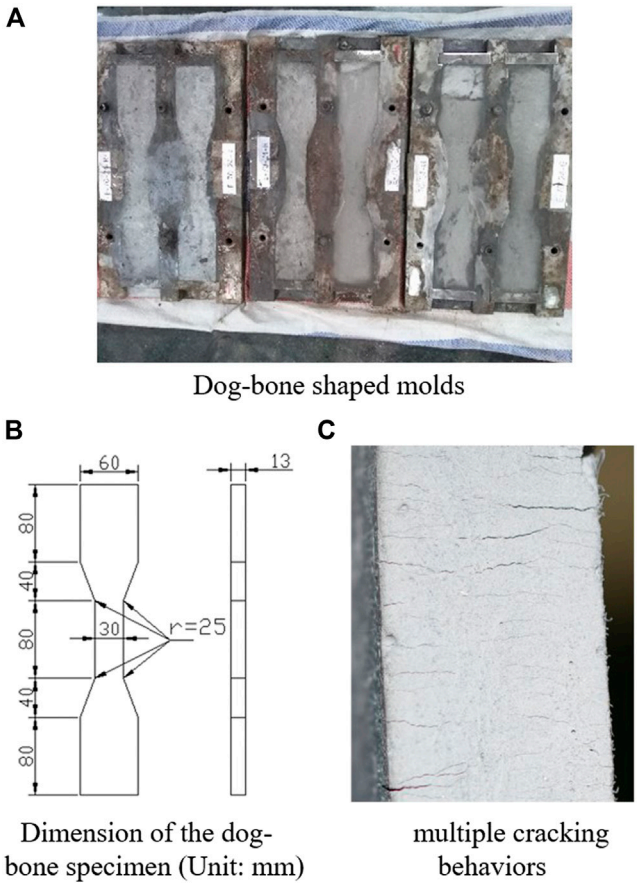

FIGURE 1 | Design and performance of the adapted ECC in the experiment.

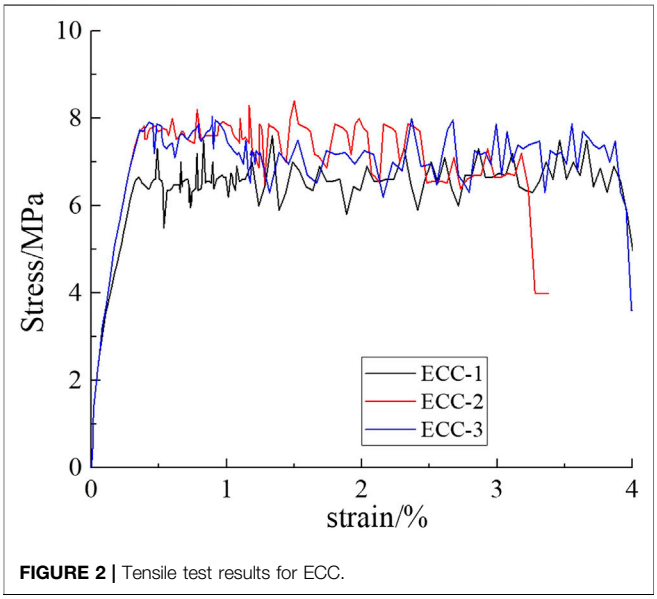

FIGURE 2 | Tensile test results for ECC.

TABLE 3 | Mechanical properties of reinforcement.

Reinforced bar	Deformed bars			Plain bars
Diameter/mm	12	16	20	16
Yield force/kN	49.39	83.38	139.43	50.84
Yield strength/MPa	436.89	415.06	444.05	252.99
Ultimate strength/MPa	590.75	556.05	653.69	388.40
Elastic modulus/GPa	181.5	181	207	211

and meet the requirements of Engineered Cementitious Composite.

The average value and standard deviation of the ultimate tensile stress of these three ECC specimens were 7.11 MPa and 0.43, respectively. If the design strength guaranteed rate was 95%, the tensile strength f_{tyk} after considering the influence of concrete standard deviation and guarantee rate was calculated as follows:

$$f_{tyk} = \mu - 1.645\sigma = 7.11 - 1.645 \times 0.43 = 6.41MPa \quad (1)$$

If the concrete material was to be used in engineering design calculation, the discreteness of the concrete material properties needed to be considered through material partial coefficient. The material partial coefficient of ECC was supposed to be 1.4, which kept the same as that of ordinary concrete. Therefore, the design value of the tensile strength of ECC concrete, namely tensile yield strength, was calculated as follows:

$$f_{ty} = \frac{f_{tyk}}{\gamma_c} = \frac{6.41}{1.4} = 4.58MPa \quad (2)$$

The diameters of the reinforcing bars in this study were 12, 16, and 20 mm, respectively. Plain rebars were used in one group and deformed rebars were used in three groups. Each group included two specimens. The material properties of these reinforcing bars were given in **Table 3**.

A normal concrete drum mixer with a volume of 30 L was used to mix constituents to produce specimens of ECC. Firstly, the dry constituents (cement and silica sand) were premixed without water in the concrete drum mixer for about 2–3 min. Secondly, the superplasticizer was dissolved in the water and was added together with the water to the mixer for 3–5 min stirring until the mortar showed good fluidity. Since the fibers can bridge micro-cracks, the dispersion of fibers in fiber-reinforced cementitious composites was a crucial factor with respect to achieving the desired mechanical performance. In this study, a demolding air pump, which

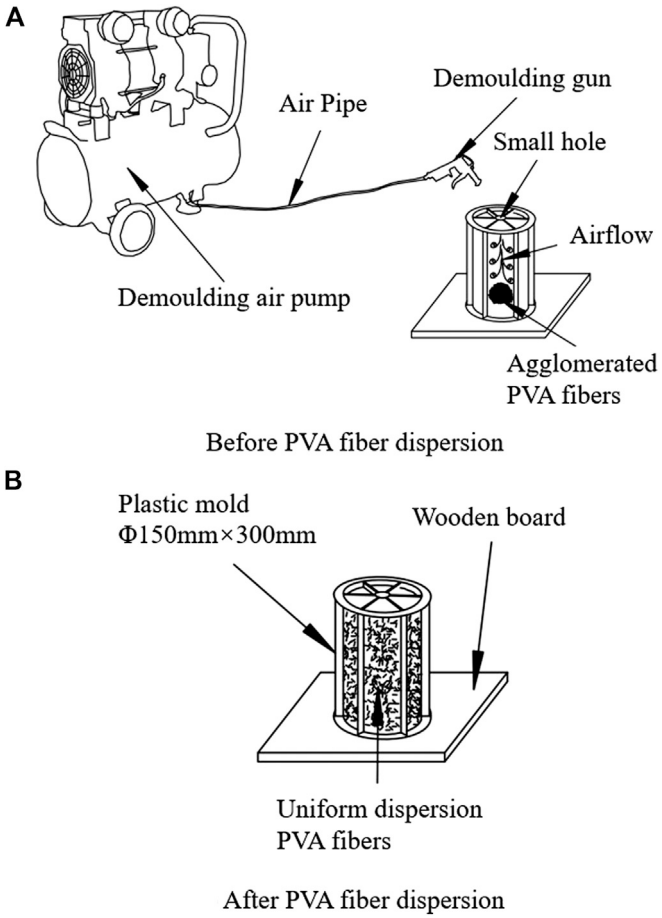

FIGURE 3 | The uniform dispersion PVA fiber by a demolding air pump.

was originally used to release concrete specimen from a plastic mold, was employed to ensure the uniform dispersion of PVA fiber. The purchased and agglomerated PVA fibers were placed on a smooth wooden board, and the plastic mold with a diameter of 150 mm and a height of 300 mm was turned upside down to cover the wooden board. A demolding gun connected to the demolding air pump by plastic air pipe was inserted into the small hole at the bottom of the plastic mold, as shown in **Figure 3A**. The lightweight PVA fibers can achieve a good uniform dispersion under the action of pressure airflow, as shown in **Figure 3B**.

The above dispersed PVA fiber was added while the mortar was stirred, and the mortar was stirred for 5–7 min until the PVA fiber was uniform dispersion for pouring. The method of casting in layers was used to avoid excessive air bubbles in the specimen due to uneven casting. When the pouring thickness reached 40–50 mm, each specimen was vibrated properly for 8–10 s on the vibrating table, and then used a putty knife to smooth the concrete layer. After casting, the concrete specimens were left in place for 24 h. Thereafter, the specimens were de-molded, marked, covered with cloth, watered and cured 2–3 times a day until the age of concrete reached 28 days, as shown in **Figure 4**.

Specimen Design

In this paper, pull-out tests were used to study the bond behavior of steel bar-ECC considering the effects of parameters such as steel bar diameter and type, cover layer thickness, embedment length and fiber volume content. A total of 45 pull-out specimens for deformed steel bar were divided into 15 groups according to different rebar diameters (20, 16, 12 mm), different rebar types (deformed rebar and plain rebar), different cover layer thicknesses (69, 72, 90 mm), different embedment lengths (100, 80, 60 mm) and different fiber volume contents (0, 1, 1.5, 2%). Each group had three identical specimens. The details of specimen parameters were listed in **Table 4**. The specimens were labeled according to their parameters. E was employed to represent engineered cementitious composite (ECC). A, B, C were used to represent embedment length from 60 to 100 mm. 12, 16, 20 were used to denote rebar diameters from 12 to 20 mm. 0, 0.5, and 1.5 were used to signify the fiber volume fraction of PVA from 0.5 to 1.5%. R was used to mean that the

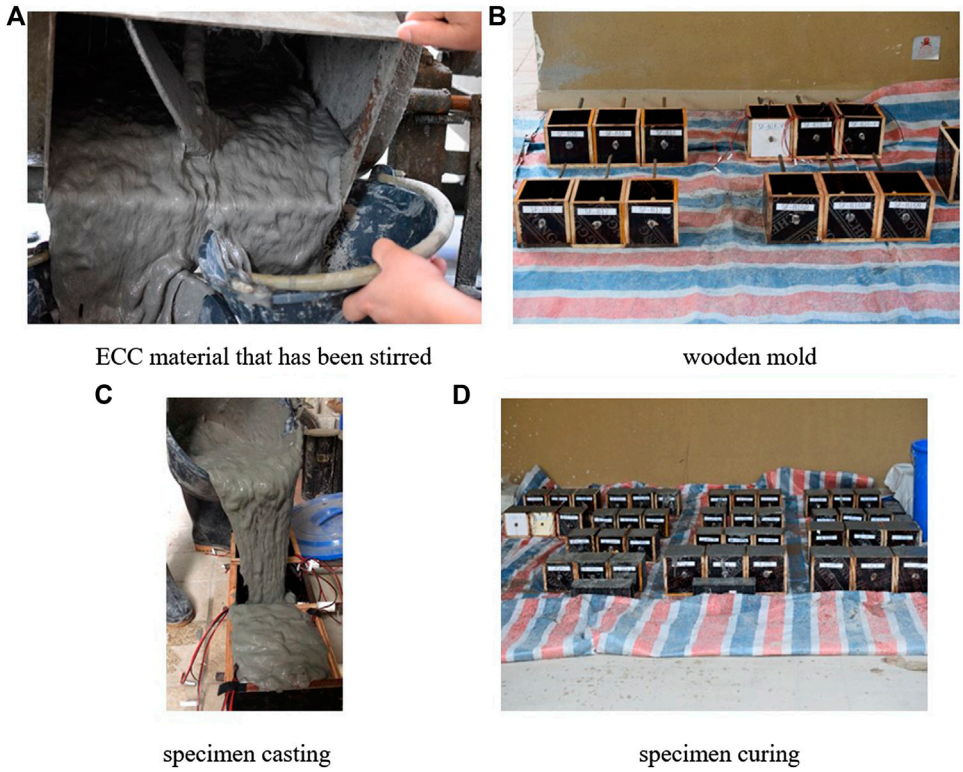

FIGURE 4 | Production process of ECC specimens.

TABLE 4 | Detailed parameters of pull-out test specimens.

Specimen code	Cube specimen edge-length/mm	Cover layer thickness/mm	Embedment length/mm	Rebar diameter/mm	Volume fraction of fiber/%
E-A12	150	69	60	12	2
E-A16	160	72	60	16	2
E-A20	200	90	60	20	2
E-A16R	160	72	60	16 (plain rebar)	2
E-B12	150	69	80	12	2
E-B16	160	72	80	16	2
E-B20	200	90	80	20	2
E-B16R	160	72	80	16 (plain rebar)	2
E-C12	150	69	100	12	2
E-C16	160	72	100	16	2
E-C20	200	90	100	20	2
E-C16R	160	72	100	16 (plain rebar)	2
E-B16–0	160	72	80	16	0
E-B16–1	160	72	80	16	1
E-B16–1.5	160	72	80	16	1.5

rebar type is plain rebar. For example, specimen E-B16R denoted pull-out test specimen with engineered cementitious composite (ECC), embedment length of 80, 16 mm-diameter plain rebar and PVA fiber fraction of 2%. Specimen E-B16–1.5 denoted pull-out test specimen with engineered cementitious composite (ECC), embedment length of 80, 16 mm-diameter deformed rebar and PVA fiber fraction of 1.5%.

Experiment Setup and Measurement

Figure 5 illustrated the schematic drawing of the specimen used in the pull-out tests. The ECC matrix of each specimen was designed to be a concrete cube with single steel reinforcement (diameter = 12, 16, or 20 mm) embedded horizontally along a central axis. The cross-sectional size (edge-length = 150, 160, or 200 mm) of the specimens were changed to accomplish varying cover layer (69, 72, or 90 mm). The unbonded segments of the pull-out specimen were created by

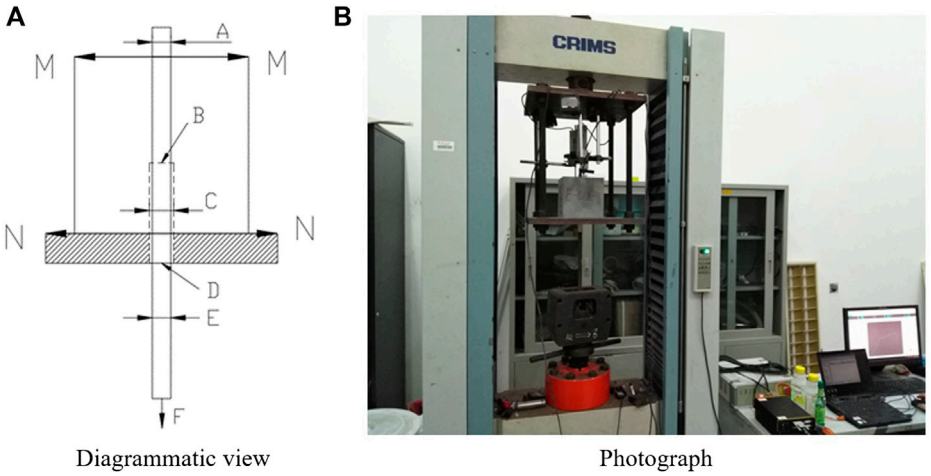

FIGURE 5 | Sketches of loading equipment and measurement location.

placing PVC pipe and the annular space between the rebar and the PVC tube was filled with polyurethane foam to avoid concrete flowing into it during the casting procedure. A 360 mm steel bar extended from the lower surface of the cube to facilitate applying pull-out load and installing linear variable displacement transducers (LVDTs), and a 50 mm steel bar was extended beyond the upper surface of the cylinder for the installation of LVDTs. The ECC concrete specimen with the embedded rebar was placed in a self-made steel frame, which was positioned in the testing machine. The frame consisted of two steel plates 25 mm thick, which were connected at the four edges with four rods 20 mm in diameter. The distance between the two steel plates was about 50 cm, so that there was enough space for installing the linear variable differential transformers (LVDTs). The top plate had a hole 30 mm in diameter in its center, allowing the rebar to run through. The pull-out load was applied using a universal test machine with a capacity of 1000kN in a displacement control mode at a rate of 0.5 mm/min until failure. The stress distribution is not constant along the embedment length of the rebar. Therefore, average bond stress τ during the pull-out test is defined as follows:

$$\tau = \frac{P}{\pi d l_a} \tag{3}$$

where P was the pull-out load, d was the rebar diameter, $l_a$was the embedment length, and P was the pull-out force. The anchorage section of the rebar was the BC segment. MM section was the surface of the concrete specimen near the free end. NN section was the surface of the concrete specimen near the loaded end, which was the contact surface between the concrete specimen and the lower steel plate of the self-made frame. Two LVDTs were placed symmetrically at the MM section and S_M represented the average of the measurements of these two LVDTs. One LVDT was installed at the free end of the rebar (AA section) to monitor its displacement S_A. The data were obtained from the TDS-530 data acquisition system. The net slip at the free end of the rebar can be calculated as follows:

$$S_F = \frac{S_A - S_M}{2} \tag{4}$$

Because the segment AB closed to the free end and the force was small, the deformation of the segment AB can be neglected during loading. But segment BF was long and close to the loaded end, the force and deformation in this section were large during loading. Therefore, the deformation of segment BF should be taken into account when calculating the net slip at the loaded end. The deformation of the rebar in segment BF can be calculated as follows:

$$\Delta S_{BF} = \frac{P}{E_S A_S} L_{BF} \tag{5}$$

where E_S was the elastic modulus of the rebar, A_S denoted the cross-sectional area of the rebar, L_{BF} refered to the initial length of the rebar in segment BF, and P was the pull-out force. If S_Z was used to represent the displacement of the testing machine loading end, the net slip at the loading end of the rebar can be calculated as follows:

$$S_L = S_Z - \Delta S_{BF} \tag{6}$$

The average relative slip between the rebar and the matrix along the anchorage section can be calculated as follows:

$$S = \frac{S_F + S_L}{2} \tag{7}$$

EXPERIMENTAL RESULTS AND DISCUSSION

Bond Stress-Slip Curves

The force transfer in the bond mechanism was generally made up of the three components, chemical adhesion, friction, and mechanical interlock between the rebar ribs and the concrete. The relationship between bond stress and slip has proved to be

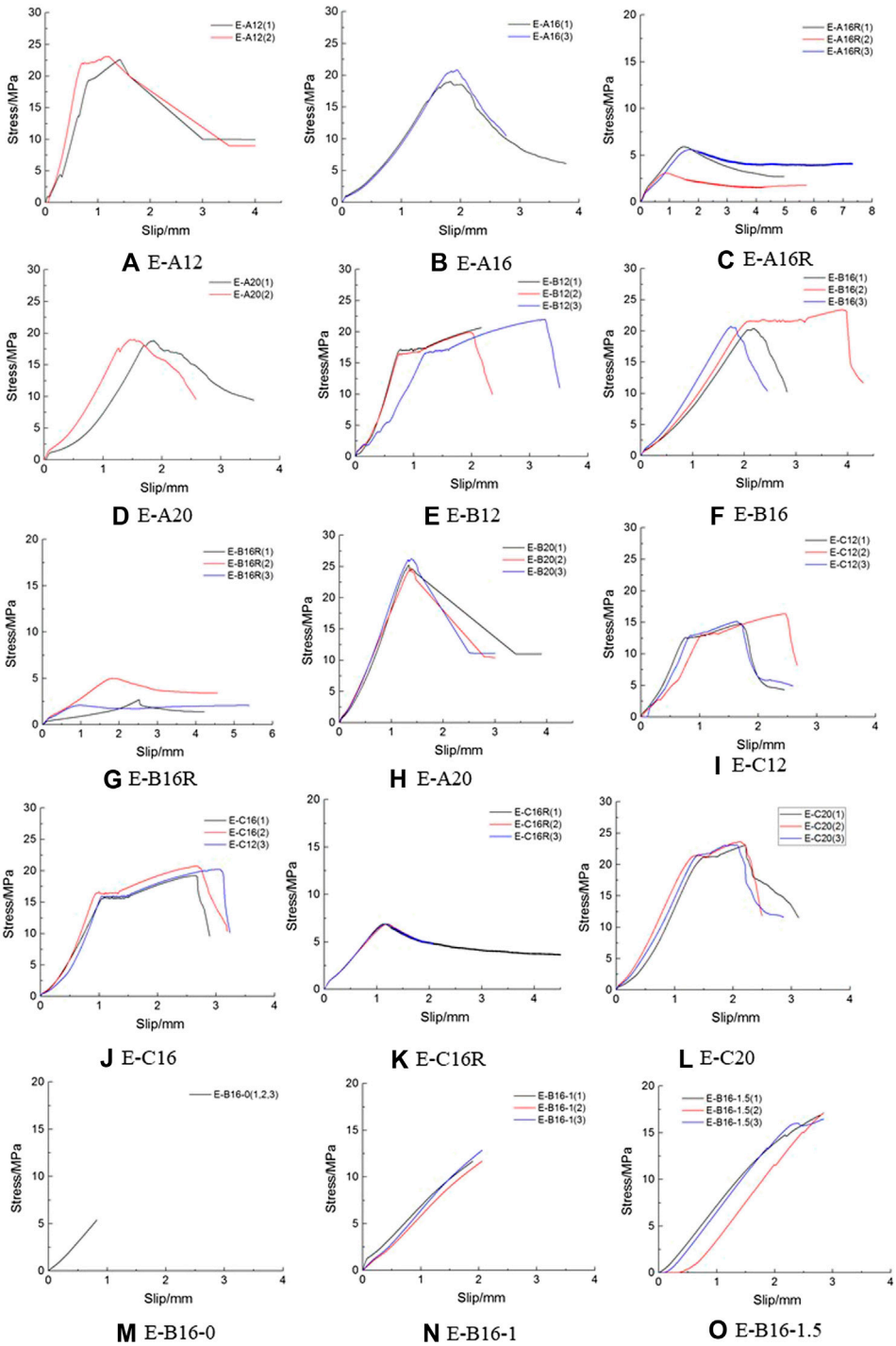

FIGURE 6 | Bond stress-slip curves.

the most effective way to study the bond behavior between reinforcement and concrete. The stress-slip relationships for this pull-out tests were shown in **Figure 6**. As the figure shows, the stress-slip curve of ECC and steel bar was similar to the stress-slip curve of normal reinforced concrete. Most of the curves can be divided into the following stages: 1) at the beginning of loading, the loading end had a slight displacement, the free end displacement was almost zero, which caused the rebars to slip slightly. The slips increased linearly with the increase of pull-out stress. The bond force between the deformed rebar, plain rebar and the concrete was mainly provided by the chemical adhesion force at this stage. 2) As the pull-out load increased, the chemical adhesion

TABLE 5 | Summary of results from steel bar-ECC unidirectional pull-out tests.

Specimen code		Ultimate pull-out load/kN	Tensile yield strength of rebar/kN	Average bond stress/MPa	Slippage/mm	Failure mode
E-A12	1	51.15	49.39	22.62	1.425	Y
	2	52.33		23.14	1.206	Y
	3*	—		—	—	—
E-A16	1	57.26	83.375	19.00	1.831	P
	2*	—		—	—	—
	3	62.79		20.83	1.938	P
E-A16R	1	17.78	50.84	5.90	1.487	P
	2	9.30		3.08	0.883	P
	3	16.89		5.60	1.723	P
E-A20	1	70.90	139.43	18.82	1.859	P
	2	71.58		19.00	1.532	P
	3*	—		—	—	—
E-B12	1	62.31	49.39	20.67	2.168	Y
	2	60.09		19.93	1.960	Y
	3	66.25		21.98	3.254	Y
E-B16	1	81.88	83.375	20.37	2.189	P
	2	94.05		23.40	3.895	Y
	3	83.18		20.70	1.741	P
E-B16R	1	10.82	50.84	2.69	2.522	P
	2	20.06		4.99	1.813	P
	3	8.42		2.09	1.006	P
E-B20	1	126.67	139.43	25.21	1.337	P
	2	124.26		24.73	1.375	P
	3	131.69		26.21	1.389	P
E-C12	1	55.48	49.39	14.72	1.694	Y
	2	61.61		16.35	2.459	Y
	3	57.21		15.18	1.636	Y
E-C16	1	96.66	83.375	19.24	2.629	Y
	2	104.28		20.76	2.670	Y
	3	101.78		20.26	3.055	Y
E-C16R	1	34.62	50.84	6.89	1.133	P
	2	18.61		3.71	1.197	P
	3	25.62		5.10	1.171	P
E-C20	1	123.17	139.43	23.08	2.213	P
	2	148.55		23.65	2.104	Y
	3	145.51		23.17	2.000	Y
E-B16–0	1	27.88	83.375	6.94	0.72	SP
	2	27.88		6.94	0.72	SP
	3	27.88		6.94	0.72	SP
E-B16–1	1	46.95	83.375	11.68	1.894	P
	2	47.02		11.70	2.054	P
	3	51.65		12.85	2.054	P
E-B16–1.5	1	67.88	83.375	16.89	2.786	P
	2	77.85		19.37	2.844	P
	3	66.84		16.63	2.845	P

P, pull-out failure; SP, splitting-pullout failure; Y, yielding failure of the steel bar.

force was gradually lost from the loaded end to the free end, which meant that the damage for debonding began from the loaded end and then transfers gradually to the free end. The chemical adhesion force disappears as a relative slip between the rebars and concrete was generated. Cracks appeared in the concrete due to the circumferential expansion force produced by the pull-out of the bars. This phenomenon accelerated the development of slip, and the force transfer mechanism relied mainly on sliding friction force. 3) Then, as the load increased further, the concrete between the threads of rebars was gradually crushed. The bond stress–slip curve exhibited a nonlinear response, and ultimately, the bond stress reached the limit. 4) As the slip of the rebars increased, the mechanical interlocking cannot resist applied load anymore and it showed a rapid reduction of load with a significant increase in slip. Cracks in the cover layer developed rapidly from inside to the outside, and the bond-stress-slip curve entered the falling stage. 5) When the load decreased to a certain value, the amount of slippage increased and the load kept fluctuating around a certain value. In this stage, the concrete in contact with the rebar became a relatively flat-concave surface. The bond stress was mainly provided by sliding friction.

Bond Failure Modes

There were mainly three types of failure modes: pull-out failure, splitting pull-out failure, and yielding failure of the steel bar. Pull-

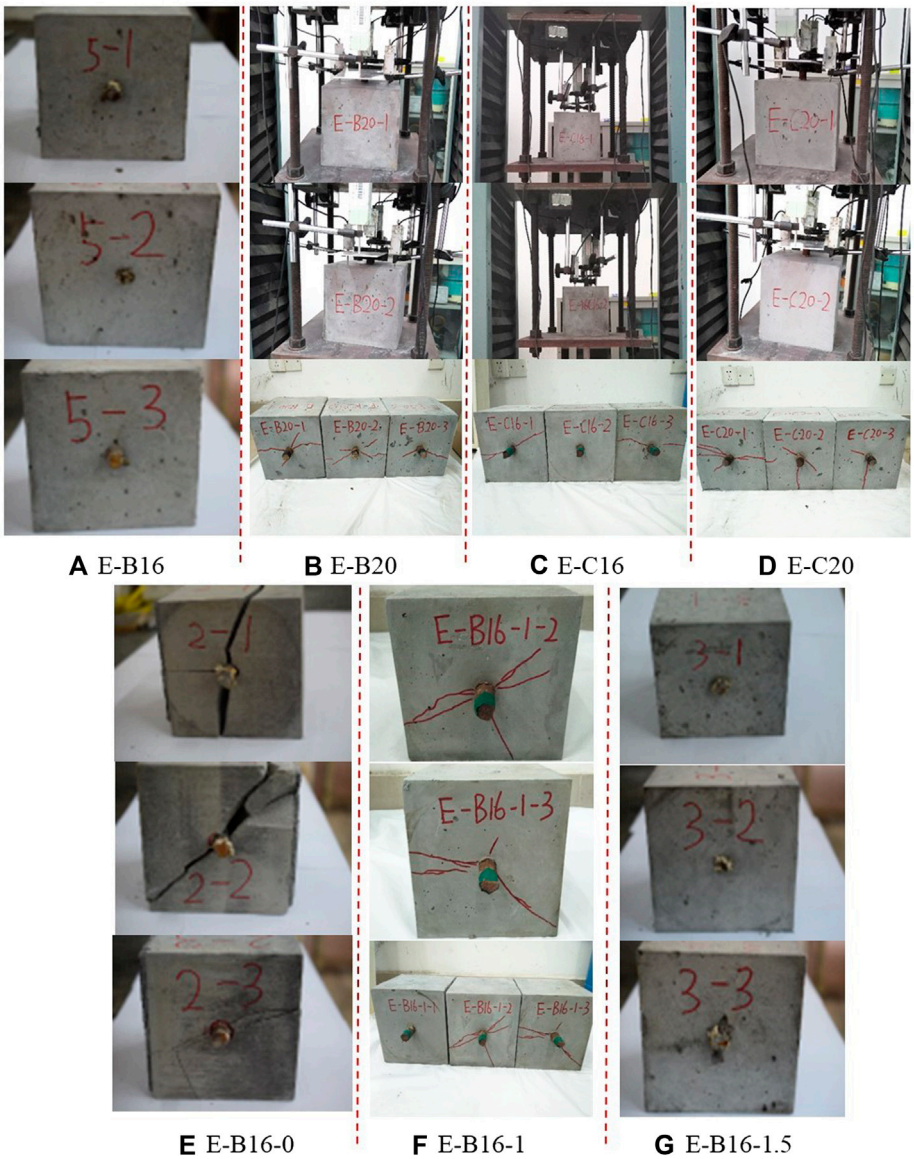

FIGURE 7 | Typical failure modes.

out failure refers to the failure mode that the steel bar was pulled out of the concrete materials due to the concrete teeth between the ribs of the deformed steel bar being sheared off. This failure mode was very common in the pull-out test of the plain steel bars embedded in concrete. Splitting pull-out failure usually occurred in the pull-out test of ribbed steel bars. The circumferential tension of the surrounding concrete would occur under the action of the radial component of the squeeze force of the steel deformed rib on the concrete, and when this force exceeded the tensile strength of concrete, the concrete cover layer would be split. Yielding failure of the steel bar referred to the failure mode where the steel bar was yielded before the bond strength between the steel bar and concrete was exceeded. The failure modes of these pull-out specimens were listed in **Table 5**, where P represented the pull-out failure mode, SP represented the splitting-pullout failure mode, and Y represented yielding failure of the steel bar. The pictures of typical failure modes were shown in **Figure 7**.

It could be seen from **Table 5** that the failure modes between ECC and steel bars were mainly pull-out failure and yielding failure of the steel bar. For the pull-out failure specimens, the steel bar had been pulled out before yielding, and at the same time, many cracks appeared on the surface of the specimen, such as specimens E-B16 and E-B20. For the yielding failure specimens, after the stress of the steel bar reaching the yield strength, the steel bar was pulled out with the increase of the force, accompanied by many cracks on the surface of the specimen, such as specimens E-C16 and E-C20.

When the embedment length of ECC concrete members was 80 mm, the bond strength showed a decreasing trend and the

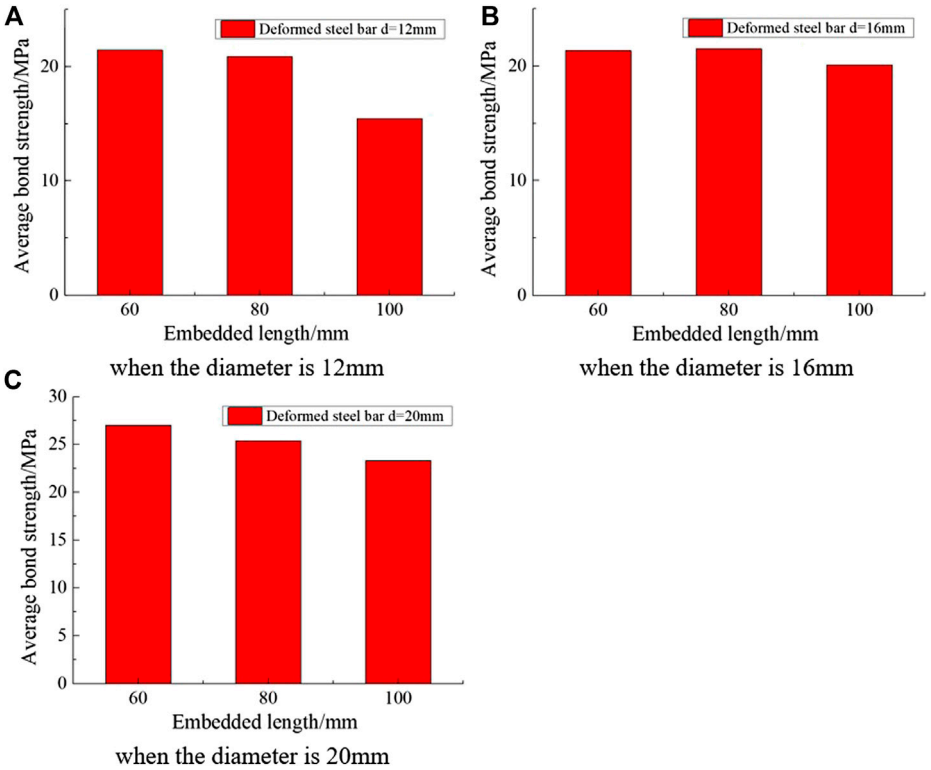

FIGURE 8 | The influence of embedded length on bond strength.

ultimate tensile force showed an increasing trend with an increase in the diameter of ribbed steel bars. The smaller the steel bar diameter, the easier the steel bar to yield. The failure modes between ECC concrete and plain steel bars were obviously pull-out failure and the bond strength was very small. For example, the measured bond strength of the specimens E-A16R, E-B16R and E-C16R were between 2 and 7 MPa.

THE EFFECTS OF PARAMETERS ON BOND BEHAVIOR

Embedment Length

Based on test recommendations in different international guidelines and standards, the bonded length was chosen to be 5 d (d is diameter of steel bar) (Solyom et al., 2020). The bonded length was sufficiently short to enable the development of a nearly uniform bond stress distribution along the embedded portion of the bar. For the convenience of comparison, the embedment lengths were designed to be 60, 80, 100, which are five times the three different diameters of the rebar (12, 16, and 20 mm) in this paper. In order to explore the influence of embedded length on bond strength, the average bond strength experimental results of the same diameter with different embedment lengths were plotted as a histogram in **Figure 8**. It was noticed from **Figure 8** that the bond strength decreased with the increase of embedded length. According to previous research, there were two possible explanations for this phenomenon. One explanation was that the confinement effect of surrounding concrete on the rebar was more severely reduced by Poisson's ratio effect when the embedment length increases because of the increased pull-out force (Shin et al., 2018). The other explanation was that as the embedment length increased, the bond stress distribution in the bonded section became increasingly nonuniform, resulting in a decrease in the average bond stress (Huang et al., 2020).

Rebar Type and Diameter

The average bond strength of Φ12 ribbed steel bars, Φ16 ribbed steel bars, Φ20 ribbed steel bars and Φ16 plain steel bars under the same embedment length were plotted as a histogram in **Figure 9**. Firstly, the bond strength of plain bars was significantly smaller than that of deformed bars. When the diameter of the rebar was 16 mm and the embedment length was 60, 80, and 100 mm, respectively, the bond strength of the plain rebar was 22.7, 15.2, and 26.1 of that of the deformed rebar. Similar to the bond action composition between other concrete and steel bars, the bond action between the plain steel bars and ECC mainly consisted of chemical adhesion, friction, and mechanical interlocking. In the initial stage of the pull-out test, the chemical adhesion between ECC and plain steel bars played a major role. The chemical adhesion disappears gradually with the generation and increase of slippage between the plain

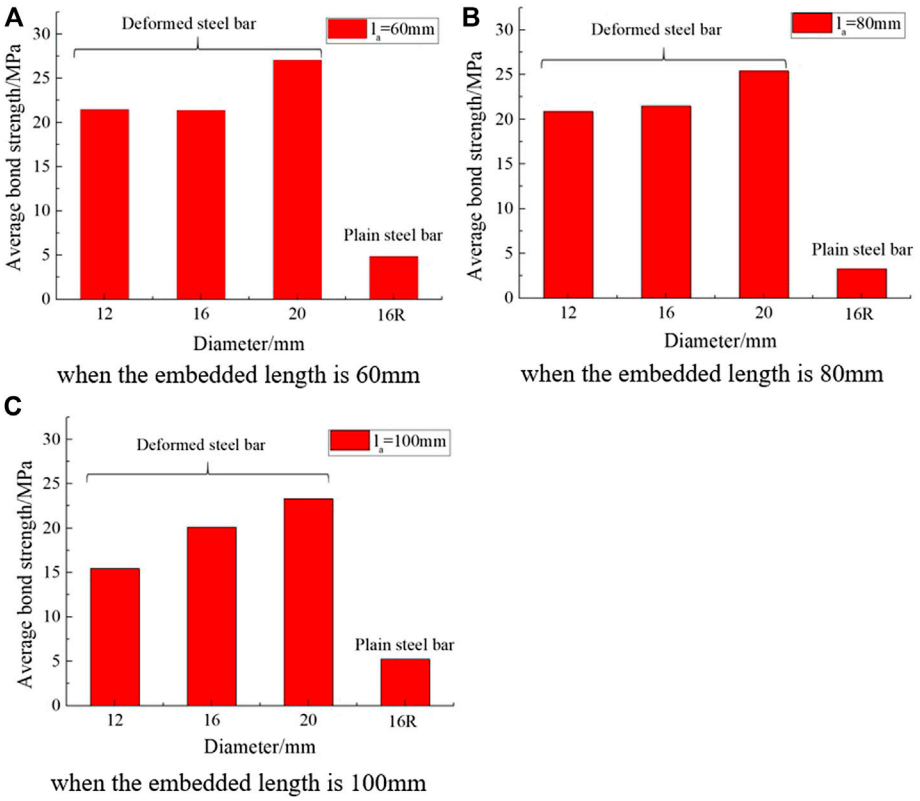

FIGURE 9 | The influence of bar diameter and the shape of the bar's surface on bond strength.

steel bars and ECC, and the friction gradually replaced the chemical adhesion to plays a major role in the later stage of the pull-out test. Since the mechanical interlocking action was almost negligible, the bond stress of plain bars was significantly smaller than that of deformed bars. When the chemical adhesion and friction were lost, the pull-out failure mode occurred. The plain steel bar would be pulled out and almost no concrete cracks would appear on the concrete surface. Compared with plain steel bars, although the initial bond action between deformed steel bars and ECC was still mainly composed by the chemical adhesion, as the relative slip between the deformed steel bars and ECC increases, the mechanical interlocking between the ribs of deformed bars and ECC played a primary role in the load transfer process.

Secondly, previous studies have shown that the bond strength showed a decreasing trend with an increase in the diameter of the steel bar. On the one hand, the increase in diameter lowered the relative bond area, which was negative to the improvement of bond development (Deng et al., 2018). On the other hand, owing to Poisson's effect, the diameter of the steel bar with larger diameter decreases more significantly when the pull-out force is larger, which led to a decreased confining pressure. As a result, lower average bond strength was obtained (Shin et al., 2018). In this case, large-diameter bars required a longer embedded length to accomplish the same bond stress. Higher bond strength would be obtained with a lower embedment length. When the diameter of the rebar changed under the same embedment length, the experimental bond strength would be larger if the embedment length was less than 5 times the diameter of the rebar. If the embedment length was greater than 5 times the steel bar diameter, the experimental bond strength would be lower. In this study, for example, as shown in **Figure 9**, when the embedded length was 60 mm, for 16 mm and 20 mm rebar, 60 mm was less than 5d of these two rebars, and the shear stress distribution within the embedded length of 16 and 20 mm steel bars was more uniform and larger than that of 12 mm steel bars. As a result, the average bond strengths of 16 mm and 20 mm rebar were greater than that of 12 mm rebar.

Protective Layer Thickness and Rebar Diameter

Studies (Wang et al., 2015; Deng et al., 2018) have shown that cover layer thickness and steel bar diameter were a critical factor that influences the average bond strength of reinforced concrete structures. Firstly, the bond strength showed a decreasing trend with an increase in the diameter of the steel bar due to the relative bond area [the ratio of the perimeter length (πd) to the cross area ($\pi d^2/4$)] and Poisson's effect. Secondly, the bond strength showed an increasing trend with an increase in the cover layer thickness. As the cover layer thickness

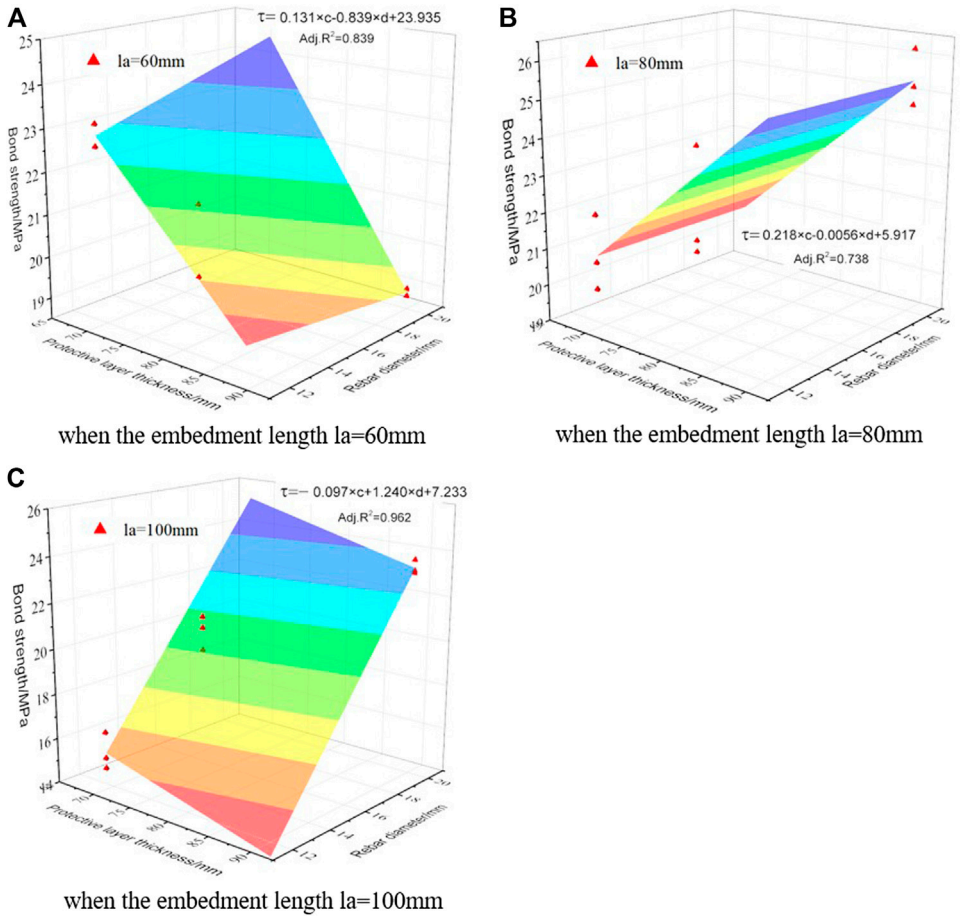

FIGURE 10 | Regression analysis between bond strength and cover layer thickness and rebar diameter.

increased, the bond strength showed an upward trend. Because the greater cover layer thickness can promote the confinement to the bar and also the shear resistance of the cementitious cover.

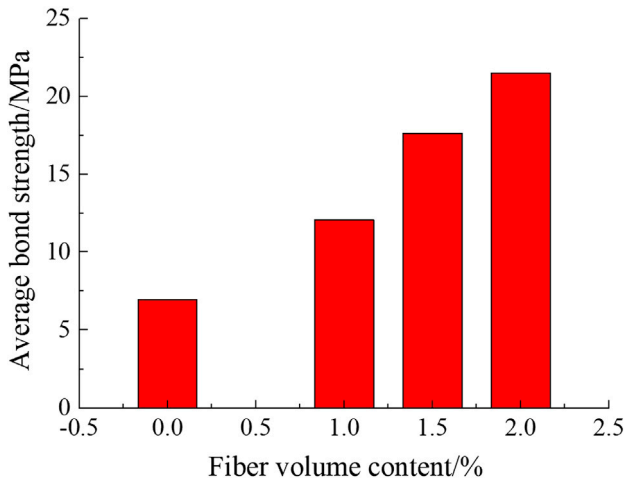

FIGURE 11 | Effect of fiber volume content on average bond strength.

In this study, cube specimens with three dimensions of 150, 160, and 200 mm were adopted and the diameters of the rebars embedded in the specimens were 12, 16, 20 mm respectively. The cover layer thicknesses were calculated to be 69, 72, 90 mm respectively. In order to explore the influence of the cover layer thickness on the bond strength, the functional relationship between bond strength and cover layer thickness and rebar diameter was assumed as follows:

$$\tau = m \times c + n \times d + q \tag{8}$$

where τ was the bond strength; c was the cover layer thickness; d was the rebar diameter; m, n and q were fitting parameters. Through regression analysis with the test data, the empirical equation of bond strength is as follows:

when the embedment length la = 60 mm, $\tau = 0.131 \times c - 0.839 \times d + 23.935$, Adj.$R^2$ = 0.839;

when the embedment length la = 80 mm, $\tau = 0.218 \times c - 0.0056 \times d + 5.917$, Adj. R^2 = 0.738;

when the embedment length la = 100 mm, $\tau = -0.097 \times c + 1.240 \times d + 7.233$, Adj. R^2 = 0.962.

The fitting plane corresponding to the empirical formula and tested data points in a three-dimensional coordinate system were

plotted in **Figure 10**. The fitted result of Adj. R2 is close to 1, which indicated that the empirical formula could make a good prediction on the test data. It can be seen from **Figure 10** that the bond strength of ECC was affected by both the steel bar diameter and the thickness of the cover layer under the same embedment length. When the embedment length la = 60 mm and la = 80 mm, the fitting parameters m = 0.131 and m = 0.218 were both greater than 0, which indicated that the bond strength increased as the thickness of the cover layer increased under these circumstances. At the same time, the fitting parameters n = −0.839 and n = −0.0056 are both less than 0, which indicated that the bond strength decreased as the diameter increased under these circumstances. However, when the embedment length la = 100 mm, the fitting parameter m was less than 0 and n was greater than 0. This was because the embedment length of 100 mm was bigger than five times the diameters for 12 and 16 mm rebars. Under these circumstances, it needed to reduce the cover layer thickness or increase the rebar diameter to fully develop the bond strength.

Fiber Volume Content

Under the condition that the steel bar diameter, cover layer thickness, embedment lengths are the same, this paper employed four groups of specimens (E-B16–0, E-B16–1, E-B16–1.5, E-B16) to investigate the effect of PVA fiber volume content (0, 1, 1.5, 2%) on bond strength, as shown in **Figure 11**. When the fiber volume content was 0% (specimen E-B16–0), the tensile strength of concrete was very low due to the lack of PVA fiber restraint. When the bond stress exceeds a certain value, which was 6.94 MPa for E-B16–0 in this paper, the bond failure would be caused by the splitting of concrete, and only 0.72 mm slippage occurs at the free end. When the fiber volume content was 1 and 1.5% (specimen E-B16–1 and E-B16–1.5), the average bond strength was 12.08 and 17.63 MPa, respectively, and the bond strength of these specimens (E-B16–1 and E-B16–1.5) were 1.5 and 2.5 times that of specimen E-B16–0, respectively. This was attributed to the bridging effect controlled the width of splitting cracks in the matrix, thereby enhancing the sliding friction force at the interface between rebar and matrix during the pull-out process. The bond strength increased obviously with the increase of fiber content. When the fiber volume content is 2% (specimen E-B16–2), the bond strength between ECC and steel bar was not only improved to be 3.1 times that of specimen E-B16–0, but also the failure mode of a specimen was transferred from pull-out failure to yielding failure of the steel bar.

CONCLUSION

This paper investigated the bond behavior of rebar embedded in engineered cementitious composite (PVA-ECC) by pull-out test and evaluated the influence of rebar diameter and type, cover layer thickness, embedment length and fiber volume content. The following conclusions can be drawn from experimental results:

1. The stress-slip curve of ECC and steel bar was similar to the stress-slip curve of normal reinforced concrete. Failure modes between ECC and steel bars were mainly pull-out failure and yielding failure of the steel bar.

2. As the embedment length increased, the bond stress distribution in the bonded section became increasingly nonuniform. The bond strength decreased with the increase of embedded length.

3. When the diameter of the rebar changed under the same embedment length, the experimental bond strength would be larger if the embedment length was less than five times the diameter of the rebar. If the embedment length was greater than five times the steel bar diameter, the experimental bond strength would be lower.

4. Through regression analysis with the test data, the functional relationships between bond strength and cover layer thickness and rebar diameter were fitted well. From the signs of the fitting parameters m and n, it indicated that when the embedment length la = 60 mm and la = 80 mm, the bond strength increases as the thickness of the cover layer increases and the bond strength decreases as the diameter increases. However, when the embedment length la = 100 mm, the signs of m and n are opposite to the previous case. This may be due to the longer embedment length so that it needs to reduce the cover layer thickness or increase the rebar diameter to fully develop the bond strength.

5. The bond strength increases obviously with the increase of fiber content. When the fiber volume content is 1, 1.5 and 2%, the bond strength of these specimens were 1.5, 2.5 and 3.1 times that of specimens without PVA fiber. This is attributed to the bridging effect controlled the width of splitting cracks in the matrix, thereby enhancing the sliding friction force at the interface between rebar and matrix during the pull-out process.

DATA AVAILABILITY STATEMENT

The original contributions presented in the study are included in the article/**Supplementary Material**, further inquiries can be directed to the corresponding author.

AUTHOR CONTRIBUTIONS

JX, XL, and HJ conceived and designed the study. YM, LL, and KZ performed the experiments. JX, YM, and HJ wrote the paper. JX, XL, and HJ reviewed and edited the manuscript. All authors contributed to the article and approved the submitted version.

FUNDING

The research presented was funded by the National Natural Science Foundation of China (51778150) and the National Natural Science Foundation of China (51808133), Natural Science Foundation of Guangdong Province in China

(2016A030313699), Guangzhou Municipal Science and Technology Project China (201804010422).

ACKNOWLEDGMENTS

The authors would like to thank the National Natural Science Foundation of China for funding this project. The laboratory of school of civil and transportation engineering at Guangdong University of Technology is also gratefully acknowledged for providing all the resources required for this work.

SUPPLEMENTARY MATERIAL

The Supplementary Material for this article can be found online at: https://www.frontiersin.org/articles/10.3389/fmats.2021.633404/full#supplementary-material.

REFERENCES

Achara, B. E., Mohammed, B. S., and Liew, M. S. (2019). Bond behaviour of nano-silica-modified self-compacting engineered cementitious composite using response surface methodology. *Construct. Build. Mater.* 224, 796–814. doi:10.1016/j.conbuildmat.2019.07.115

Baena, M., Torres, L., Turon, A., and Barris, C. (2009). Experimental study of bond behaviour between concrete and FRP bars using a pull-out test. *Compos. B Eng.* 40 (8), 784–797. doi:10.1016/j.compositesb.2009.07.003

Bai, L., Yu, J. P., Zhang, M., and Zhou, T. H. (2019). Experimental study on the bond behavior between H-shaped steel and engineered cementitious composites. *Construct. Build. Mater.* 196, 214–232. doi:10.1016/j.conbuildmat.2018.11.117

Cai, J. M., Pan, J. L., Tan, J. W., and Li, X. P. (2020). Bond behaviours of deformed steel rebars in engineered cementitious composites (ECC) and concrete. *Construct. Build. Mater.* 252, 12. doi:10.1016/j.conbuildmat.2020.119082

Chao, S. H., Naaman, A. E., and Parra-Montesinos, G. J. (2009). Bond behavior of reinforcing bars in tensile strain-hardening fiber-reinforced cement composites. *ACI Struct. J.* 106 (6), 897–906.

Deng, M. K., Pan, J. J., and Sun, H. Z. (2018). Bond behavior of steel bar embedded in Engineered Cementitious Composites under pullout load. *Construct. Build. Mater.* 168, 705–714. doi:10.1016/j.conbuildmat.2018.02.165

Hossain, K. M. A., Alam, S., Anwar, M. S., and Julkarnine, K. M. Y. (2020). Bond strength of fibre-reinforced polymer bars in engineered cementitious composites. *Proc. Inst. Civ. Eng.-Constr. Mater.* 173 (1), 15–27. doi:10.1680/jcoma.17.00020

Huang, H., Yuan, Y. J., Zhang, W., Hao, R. Q., and Zeng, J. (2020). Bond properties between GFRP bars and hybrid fiber-reinforced concrete containing three types of artificial fibers. *Construct. Build. Mater.* 250, 18. doi:10.1016/j.conbuildmat.2020.118857

Jiang, H., Wei, R., Ma, Z. J., Li, Y., and Jing, Y. (2016). Shear strength of steel fiber-reinforced concrete dry joints in precast segmental bridges. *J. Bridge Eng.* 21 (11), 04016085. doi:10.1061/(asce)be.1943-5592.0000968

Kim, B., and Lee, J. Y. (2012). Polyvinyl alcohol engineered cementitious composite (PVA-ECC) for the interfacial bond behaviour of glass fibre reinforced polymer bars (GFRP). *Polym. Polym. Compos.* 20 (6), 545–557. doi:10.1177/096739111202000605

Lee, S. W., Kang, S. B., Tan, K. H., and Yang, E. H. (2016). Experimental and analytical investigation on bond-slip behaviour of deformed bars embedded in engineered cementitious composites. *Construct. Build. Mater.* 127, 494–503. doi:10.1016/j.conbuildmat.2016.10.036

Li, V. C. (2019). *Engineered cementitious composites (ECC): bendable concrete for sustainable and resilient infrastructure*, Germany: Springer-Verlag Berlin Heidelberg.

Li, X. L., Bao, Y., Xue, N., and Chen, G. D. (2017). Bond strength of steel bars embedded in high-performance fiber-reinforced cementitious composite before and after exposure to elevated temperatures. *Fire Saf. J.* 92, 98–106. doi:10.1016/j.firesaf.2017.06.006

Ma, Y., Guo, Z., Wang, L., and Zhang, J. (2017). Experimental investigation of corrosion effect on bond behavior between reinforcing bar and concrete. *Construct. Build. Mater.* 152, 240–249. doi:10.1016/j.conbuildmat.2017.06.169

Nguyen, H. A., Chang, T. P., Lee, P. H., and Shih, J. Y. (2020). Experimental investigation of bond-slip performance of reinforcement in two green concretes. *J. Mater. Civ. Eng.* 32 (3), 7. doi:10.1061/(asce)mt.1943-5533.0003029

Pauletta, M., Rovere, N., Randl, N., and Russo, G. (2020). Bond-slip behavior between stainless steel rebars and concrete. *Materials* 13 (4), 17. doi:10.3390/ma13040979

Rockson, C., Tamanna, K., Alam, M. S., and Rteil, A. (2020). Effect of cover on bond strength of structural concrete using commercially produced recycled coarse and fine aggregates. *Construct. Build. Mater.* 255, 16. doi:10.1016/j.conbuildmat.2020.119275

Shin, H.-O., Lee, S.-J., and Yoo, D.-Y. (2018). Bond behavior of pretensioned strand embedded in ultra-high-performance fiber-reinforced concrete. *Int. J. Concr. Struct. Mater.* 12 (1). doi:10.1186/s40069-018-0249-4

Solyom, S., Di Benedetti, M., Guadagnini, M., and Balazs, G. L. (2020). Effect of temperature on the bond behaviour of GFRP bars in concrete. *Compos. B Eng.* 183, 10. doi:10.1016/j.compositesb.2019.107602

Wang, H. L., Sun, X. Y., Peng, G. Y., Luo, Y. J., and Ying, Q. M. (2015). Experimental study on bond behaviour between BFRP bar and engineered cementitious composite. *Construct. Build. Mater.* 95, 448–456. doi:10.1016/j.conbuildmat.2015.07.135

Wang, L., Guo, F., Yang, H., Wang, Y., and Tang, S. (2020b). Comparison of FLY ASH, PVA fiber, mgo and shrinkage-reducing admixture on the frost resistance of face slab concrete via pore structural and fractal analysis. *Fractals* doi:10.1142/s0218348x21400028

Wang, L., Jin, M., Guo, F., Wang, Y., and Tang, S. (2020c). Pore structural and fractal analysis of the influence of FLY ASH and silica fume on the mechanical property and abrasion resistance of concrete. *Fractals* doi:10.1142/s0218348x2140003x

Wang, L., Jin, M., Wu, Y., Zhou, Y., and Tang, S. (2021). Hydration, shrinkage, pore structure and fractal dimension of silica fume modified low heat Portland cement-based materials. *Construct. Build. Mater.* 272, 121952. doi:10.1016/j.conbuildmat.2020.121952

Wang, L., Luo, R., Zhang, W., Jin, M., and Tang, S. (2020a). Effects of fineness and content of phosphorus slag on cement hydration, permeability, pore structure and fractal dimension of concrete. *Fractals* doi:10.1142/s0218348x21400041

Xiao, J., Qu, W., Li, W., and Zhu, P. (2016). Investigation on effect of aggregate on three non-destructive testing properties of concrete subjected to sulfuric acid attack. *Construct. Build. Mater.* 115, 486–495. doi:10.1016/j.conbuildmat.2016.04.017

Xiong, Z., Wei, W., Liu, F., Cui, C., Li, L., Zou, R., et al. (2021). Bond behaviour of recycled aggregate concrete with basalt fibre-reinforced polymer bars. *Compos. Struct.* 256, 113078. doi:10.1016/j.compstruct.2020.113078

Yu, K. Q., Ding, Y., Liu, J. P., and Bai, Y. L. (2020a). Energy dissipation characteristics of all-grade polyethylene fiber-reinforced engineered cementitious composites (PE-ECC). *Cement Concr. Compos.* 106, 11. doi:10.1016/j.cemconcomp.2019.103459

Yu, K. Q., Lu, Z. D., Dai, J. G., and Shah, S. P. (2020b). Direct tensile properties and stress-strain model of UHP-ECC. *J. Mater. Civ. Eng.* 32 (1), 13. doi:10.1061/(asce)mt.1943-5533.0002975

Zhang, J. Z., Bian, F., Zhang, Y. R., Fang, Z. F., Fu, C. Q., and Guo, J. (2018). Effect of pore structures on gas permeability and chloride diffusivity of concrete. *Construct. Build. Mater.* 163, 402–413. doi:10.1016/j.conbuildmat.2017.12.111

Zhou, Y., Fu, H., Li, P., Zhao, D., and Li, L. (2019). Bond behavior between steel bar and engineered cementitious composite (ECC) considering lateral FRP confinement: test and modeling. *Compos. Struct.* 226, 111206. doi:10.1016/j.compstruct.2019.111206

Zhou, Z., and Qiao, P. (2018). Bond behavior of epoxy-coated rebar in ultra-high performance concrete. *Construct. Build. Mater.* 182, 406–417. doi:10.1016/j.conbuildmat.2018.06.113

Conflict of Interest: Author XL and MY were employed by Yuexiu Transport Infrastructure Co., Ltd.

The remaining authors declared that the research was conducted in the absence of any commercial or financial relationships that could be construed as a potential conflict of interest.